Spring 2020

The Origins of Phantom Partials in the Piano

Lauren M. Neldner
Rollins College, lneldner@rollins.edu

THE ORIGINS OF PHANTOM PARTIALS IN THE PIANO

Lauren M. Neldner

A Senior Honors Project Submitted in Partial Fulfillment

of the Requirements of the Honors Degree Program

March 2020

Faculty Sponsor: Thomas R. Moore

Rollins College

Winter Park, FL

Contents

List of Figures

Acknowledgments

I want to thank Dr. Moore for sponsoring this thesis research and the two and half years of research that led to this point. I would also like to thank Eric Rokni for being my research partner on the projects preceding this thesis, as well as Jade Case for assisting with execution and analysis of these experiments. Finally, thank you to the rest of the physics department, my friends and family.

Chapter 1

Introduction

For the past three centuries, the piano has been considered one of the most important string instruments in the music industry. Today, many people are familiar with both the grand and upright pianos that are widely used across the world in concert halls and households alike. Significant research has been conducted in an effort to understand the intricacies that make the piano sound complex and unique and several references detail the history of the piano. Most of the information in this chapter is considered common knowledge within the scientific community, but a significant amount of the information can be found in Refs. [1] and [2].

1.1 History of the Piano

Prior to the 18th century, the two most common keyboard instruments were the clavichord and harpsichord. These instruments date back to the 1400s and were popular in the Baroque era. The clavichord is rectangular in shape and uses a tangent mechanism, which moves up to strike a string when a key is depressed. This sound can be sustained as long as the key is pressed. However, a fundamental limitation of the instrument is that the volume of the sounds produced is low and thus the instrument is not ideal for performance.

The harpsichord has a shape similar to a modern grand piano and utilizes a plucking

method to produce sound. When a key is depressed, the jack system moves up and the string is plucked. The string will continue to vibrate with a natural rate of decay until the key is released, at which point the damper falls back to it's initial resting position on the string. The primary issue with this instrument is the lack of volume control by the performer. While the instrument can be set to either produce loud or soft sounds, the individual loudness of each note cannot be controlled. Significant effort was expended to create an instrument to solve these issues.

Bartolomeo Cristofori is credited with being the first to design and build what would become the modern piano around 1700. Cristofori's ingenious design solved both problems present in the clavichord and harpsichord. He designed an action system in which leather hammers were used to strike the strings. He also designed an escapement mechanism, which enabled the hammer to hit the string and immediately rebound whether the player held the key down or not. Furthermore, he added a "back check," which catches the hammer so that it cannot strike the string more than once. To stop the string motion, he installed a damper for every key that rests on the strings until the key is depressed. When a key is pressed the damper rises and remains above the string until the key is released and it returns to its resting position on the string.

Some of the other important aspects that Cristofori included in his design were using strings with roughly twice the tension of ones used in harpsichords. To account for the added tension, the diameter of the strings was also nearly doubled and extra bracing was added to the case. Additionally, an *una corda* mechanism was installed. This piece could be hand-shifted in order to force the hammer to only strike one of the multiple strings associated with each key. This mechanism made the resulting sound softer, slightly modified the timbre of the note, and is still used in modern pianos under the colloquial name, the "soft pedal."

This new instrument by Cristofori solved the problem of being able to play both loud and soft and gave musicians control over the volume of each note they played. For this reason, Cristofori originally named the new instrument *gravecembalo col piano e forte*, which

translates as "large keyboard instrument with soft and loud." Over time the name was shortened to *pianoforte* and then further reduced to *piano*, as it is referred to today.

The piano evolved over the next two centuries. One of the most significant changes was the expansion of the musical range. Cristofori's original designs only called for 4 or $4\frac{1}{2}$ octaves, but by the mid-1800s the range had grown to $7\frac{1}{3}$ octaves, or 88 notes, which is standard for most modern pianos. Another important development stemmed from the necessity for pianos to produce more sound. This required heavier strings, which required heavier hammers. In turn, the case and frame also needed to be strengthened to accommodate the added tension, which led to the development of the metal frame in the mid-19th century. The last significant change was the development of the upright piano to accommodate the desires of the middle class consumers of the 19th century. The 20th century saw few changes to the piano other than the introduction of the baby grand piano and the miniature upright piano after the United States 1930s economic depression. With the more affordable and space conscious versions, pianos became household staples in much of Europe and America and few changes have been made to the designs since.

1.2 The Modern Piano

Pianos have been in common use throughout the 20th and 21st centuries. The general consensus is that the grand piano is superior to the upright piano and is therefore typically used for concert performance. In contrast, the upright was designed to conserve space and be used in homes and practice studios. The grand piano has the distinct advantage that it has room for longer strings, which can have greater tension and thus produce more sound. As well, because the hammers are positioned below the keys, they can utilize gravity to return to their resting position as opposed to springs.

Grand pianos range from about 6 to 9 feet long, while the term baby grand is used to refer to any piano of length less than 6 feet. The standard upright piano ranges in height

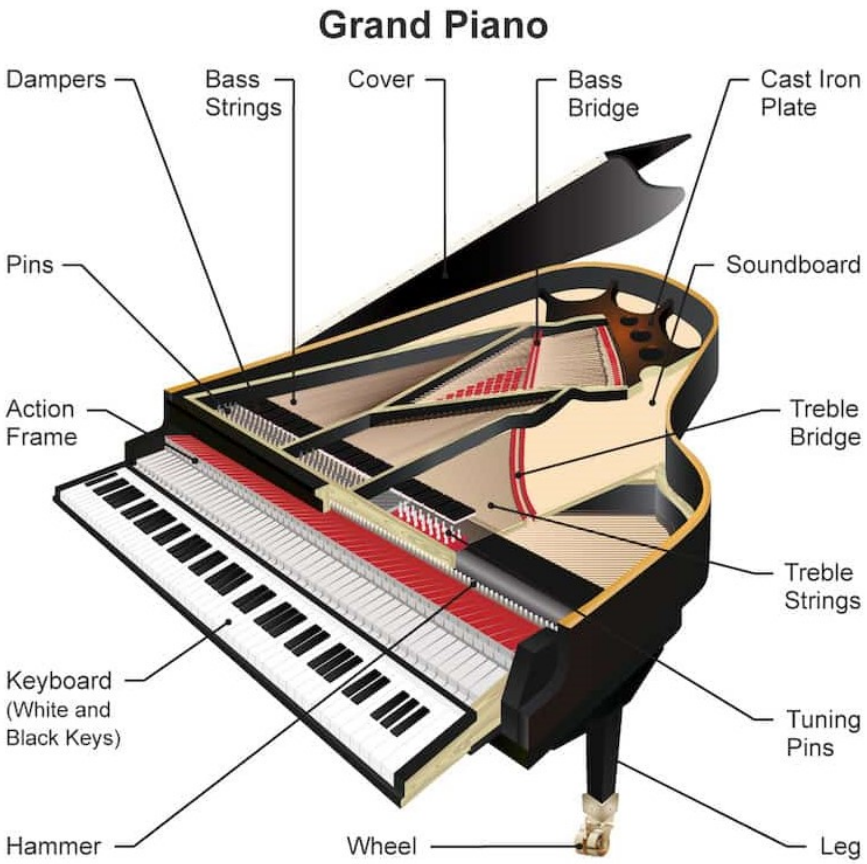

Figure 1.1: Labeled diagram of a grand piano. [3]

from 4-5 feet, however, there are miniature models which stand less than 3 feet tall. The range of modern pianos varies from $7\frac{1}{4}$ octaves to 8 octaves, depending on the model, and has a wide dynamic range.

The process of producing sound begins when the player presses down on a key and causes a hammer to strike the string or strings associated with that key. Once struck, the strings vibrate and this energy is transferred through the bridge to the soundboard. The soundboard vibrations then cause the surrounding air to be compressed, which results in the sound that is heard by the audience. The following sections provide a brief description of each component of the piano. The majority of the information is derived from three serial works by Conklin. [4–6]

1.2.1 Frame and Case

In the early 1700's, Cristofori used a wooden frame to support the piano mechanisms and string tension. The 54 strings were believed to have exerted a force of approximately 7500 N on the frame. As more keys, triple strings, and wound bass strings were added, the force increased dramatically and required a new frame design. The modern frame of the grand piano is made from cast iron to withstand the immense force exerted by the strings. In the modern piano, the over 200 strings exert approximately 150,000 Newtons (approximately 33,000 lbs) on the frame.

The case of the grand piano is made of hard wood to provide a solid casing for all of the internal components. Typically, one long strip of approximately 8-9 cm thick laminated maple is used to construct the case and can weigh several hundred pounds. Similar to the frame, it is important that the case has a large mechanical impedance to prevent vibrations from the soundboard efficiently transferring to the case. [7] The lid of a grand piano serves to increase radiation efficiency of low and medium range frequencies. Together, the case and lid direct the sound coming from the soundboard towards an audience in line with the opening of the lid.

It is important to note that all of the structural components have resonances that will be excited as a result of the string vibrating. However, work conducted by Tan et al. in 2018 was able to show that the soundboard is the dominate contributor to sound production except at high frequiencies (notes A6 and above) when the lid of the piano is the main contributor. [8]

1.2.2 Soundboard

The soundboard serves to amplify the sound produced by the strings. In most pianos, Sitka spruce or red spruce are used to construct the soundboard. Long strips of spruce 10-20 cm wide are glued together along the grain and then cut to fit in the case. Typically, the center of the soundboard is approximately 9 mm thick and tapers off toward the edge where it is

approximately 6 mm thick. When first placed into the piano the soundboard is crowned, however, due to the force exerted by the strings the soundboard flattens until there is only a slight curvature. The exact amount of crowning varies and has an effect on the balance between the radiation efficiency of high and low frequencies. Additionally, most soundboards are varnished, which helps protect against the absorption of moisture and improves tuning stability. The flattening of the soundboard and the deformation of the wooden pieces due to moisture are two of the most common problems that pianos have as a result of age, in addition to rusting of the strings and infestation with bugs or rodents.

To provide additional support to the soundboard, long pieces of hard wood, called ribs, are placed on the underside of the soundboard. These ribs are placed perpendicular to the grain and support the spruce along its weaker direction. Chaigne showed that slight differences in the spacing of the ribs can have a significant effect on the resonance of the soundboard. [9] This is a result of the influence that the ribs and bridges have on the modal structure. [10] Furthermore, the orientation of the soundboard with respect to the case and bridges is important in determining the final sound quality.

The grain of the soundboard is oriented diagonally to the direction of the case and approximately parallel to the direction of the treble bridge. Typically, the grain forms a 30-50 degree angle with the direction of the base bridge.

Studies have shown that the mechanical impedance, defined as the resistance to motion of the structure when a harmonic force is applied at the driving point, depends on frequency and can significantly effect the sound produced. [5] Furthermore, work conducted by Moore and Zietlow demonstrated that the modal shapes and resonant frequencies of the soundboard can be affected by the amount of force placed on the soundboard by the strings. [10]

The unique shape and properties of the soundboard present many challenges when attempting to model the piano. Many researchers have studied the vibro-acoustic behavior of the soundboard and attempted to build a complete model. Work towards a complete model began with Suzuki in 1986 [11] quickly followed by Kindel and Wang [12], Conklin [5]

and Giordano [13, 14]. In the 2000s, investigations by Berthaut et al. [15], Ege et al. [16], Boutillon and Ege [17] and Chabassier et al. [18] have come increasingly close to fully describing the instrument. The most recent works include a modal analysis of the grand piano by Corradi et al. [19] and a model for an upright piano soundboard by Trevisan et al. [20]

1.2.3 Bridges

To transfer energy from the strings to the soundboard, there must be a point of termination of the strings and a connection between the two components. The treble and bass bridges, typically made from either solid or laminated hard-wood, serve this purpose. Both bridges are placed on the upper side of the soundboard and the bass bridge is raised a few centimeters above the treble bridge. This overlapping of the two bridges has the distinct advantage that the bass strings can be longer while still conserving space, and the strings are all more centrally located over the soundboard, which improves the resonance and sound quality.

The primary purpose of the bridge is to couple the strings to the soundboard. The vibrations of the string transfer to the bridge, which causes it to move in all three dimensions. The transverse motion of the bridges accounts for the majority of the power in the piano sound, however, the other motions contribute non-trivial amounts of energy and thus must be included in models. Furthermore, Giordano and Korty were able to show that the longitudinal motion of the string couples to the transverse motion of the bridge. [21] Reference [5] also details the importance of the bridge design in creating the best sound quality.

The bridges present a higher impedance to the strings than if the strings were connected directly to the soundboard. The difference in the impedance of the string and bridge largely determines the loudness, duration, and quality of the sound produced and can be modified by altering the design of the bridges.

1.2.4 Strings

In the modern piano, there are 88 keys, 52 white and 36 black. The higher notes have three short, small diameter strings while most notes below B_2 are double, larger diameter wrapped strings. The lowest octave on the piano has only a single large diameter wrapped string per key. The strings are typically made from high carbon steel and the wound strings are wrapped in a copper casing.

At the far end of the grand piano, the strings are held by the hitch pins attached to the iron frame. At the other end, near the keys, they are held by the tuning pins. One end of the steel tuning pins is threaded and inserted into the pin block, which is supported by the frame, and the other end is shaped to fit a tuning key. The pin block must be made of strong enough wood to support the high stress imposed by the string and be able to resist movement from the pins slipping. In most pianos, maple is used to make the pin block.

While it may be assumed that every string associated with a single key should be tuned to the same frequency, a study conducted by Kirk found that professional tuners often tune the multiple strings to be slightly out of unison, which results in some beating against one another. [22] The study further found that both trained and amateur listeners preferred the slight deviation in tuning between the strings than perfect unison tuning. This difference in frequency of vibration has a significant impact on the bridge motion. When the frequencies are in phase, the bridge moves more and transfers energy more effiently. Weinrich showed how this led to the "double decay," or the intial fast decrease in sound amplitude followed by a much slower decay of the intensity of a note. [23]

The speaking length of the string, or the effective length of vibration, is defined by the bridges at the far end of the piano and either the capo d'astro bar or an agraffe near the keys. The capo d'astro bar is a metal plate running over the D_5 strings and above. An agraffe is a metal stud that each lower string passes through. Both the capo d'astro bar and agraffe serve the same purpose of providing string support and controlling the speaking length.

It has been known for over one hundred years that the overtones of the piano strings

do not align with the harmonics of the fundamental frequencies. The inharmonicity is particularly pronounced in the wrapped bass strings. For some strings, the higher partials can differ from the harmonics by two whole steps. [24] This phenomenon is a result of the stiffness of the piano strings. Reference [24] provides an analytical approach to describe these overtone frequencies. This fact is important to the understanding of the work presented in the following sections.

Motion of the strings

When the string is struck by the hammer, three types of motion result and all are important to the sound that is produced. The most obvious and understood motion is the transverse motion of the string. When the hammer strikes the string, a transverse wave propogates the length of the string to the bridge and the bridge couples the string to the soundboard allowing the sound to be heard. Most of the vibrational energy is reflected due to the impedance mismatch between the bridge and the string, causing the impulse to progate up and down the string resulting in a standing wave. The energy in the standing wave is slowly transferred to the soundboard via the bridge. Studies have shown that the transverse motion of the string is both perpendicular and parallel to the soundboard and each of these motions affect the sound in a slightly different way because the bridge has a different impedance depending on the direction of motion. [23]

The second type of string motion is known as the free-response longitudinal motion. The initial hammer strike induces a longitudinal standing wave in the string. These waves occur at the longitudinal resonance frequencies of the string which are characterized by both the speed of sound in the string material and the length of the string. [25] The velocity of this wave is approximately ten times faster than that of the transverse wave and thus has been shown to act as a precursor to the transverse motion and affect the transient sound. [21]

The third motion of the string is referred to as a forced-response longitudinal motion. These waves are generated due to the stretching of string that is a result of the transverse

displacement of the string. [26] As the string moves out of plane, the string is forced to elongate and compress. This motion produces frequencies that are found at the harmonics of the transverse motion as well as at their sum and difference frequencies. Due to the inharmonic overtones attributable to the stiffness of the string, these frequency components do not align with the harmonics of the transverse motion of the string. The theory of this type of string motion is elaborated on in Section 2.2. Understanding this motion is important to understanding the theory of phantom partials.

1.2.5 Hammers and Action

Piano hammers have been modified since the 18th century but in many ways are still similar to those used by Christofori. All hammers have a wooden core that is covered by layers of material that is soft and compressible. Originally leather was used as the outer layers, but during the 1800s most piano makers switched to felt. One design element that remains unchanged is that multiple layers of material are used and the outer-most layer is always the softest. Another commonality is that the bass hammers are larger and heavier than the treble hammers. This is because more force is required to make the bass strings vibrate with the same amplitude as the treble strings. However, all of the hammers are larger and heavier in the modern era as a result of increased string tension.

The hammers are connected to the keys by the mechanical mechanism known as the action. The modern action was adapted and modified from Cristofori's original design over the course of approximately a century until it was largely finalized in the mid-1800s. Many of Cristofori's original mechanisms are still in place but the modern action is much more intricate, creating added sensitivity to touch and regulation of the response of the hammers.

The interaction between the hammer and string has been studied extensively due to its direct impact on the sound produced. Felt is a complicated material to study, which makes understanding the interaction between hammer and string difficult. Multiple studies have found that the relationship between applied force of the hammer and compression of the felt

exhibits hysteristic behavior. [27] Additionally, small adjustments to the hammer felt can have a significant impact on the spectrum produced by each string. [28, 29] There can be up to a 10 dB difference in the power of the partials produced between a "too soft" hammer strike and a "too hard" hammer strike.

The velocity at which the hammer strikes the strings is also important to the sound quality. Four to five meters per second seems to be the optimal speed. Birkett recently conducted a complete analysis of the string motion induced by the hammer strikes for one to three meters per second velocities. [30]

1.2.6 Pedals and Dampers

Over time, the dampers were modified to improve functionality and three pedals were added to increase the musical capabilities of the instrument. The dampers are made from wood and have a wool covering. They rest on top of the strings at all times until the key is pressed. As the key is depressed the action system raises the damper, and when the key is released gravity brings the damper back to its resting position. The extreme upper register of the piano, typically above F_6, does not have any dampers because the natural decay of the sound is significantly more rapid than for the lower notes.

Modern pianos use three pedals to add sound variability. From left to right the peddles are the una corda pedal (also known as the soft pedal), the sostenuto pedal, and the sustaining pedal. In a modern piano the soft pedal moves the entire action and keyboard slightly to the right so that one less string is struck when a key is pressed. This produces a sound with lower volume because one less string is contributing to the total vibrations transferred to the soundboard and a softer portion of the hammer is striking the strings. Alternatively, this pedal can be used to raise the entire action so that the strings are closer to the hammers. This results in less energy being transferred to the strings, which results in less sound being produced.

The sustaining pedal works by raising every damper simultaneously. This allows for each

string to vibrate even when the keys are not pressed. Therefore, when a key is pressed and released, the strings will exhibit a natural decay of vibration and the other strings can function as sympathetic resonators. The last pedal, the sostenuto pedal, is not found on every piano but when it is included, it is typically placed in the middle of the other two. This pedal is similar to the sustaining pedal but only keeps the dampers raised for the individual keys that are currently depressed when the pedal is engaged. Thus only those few strings will continue vibrating when the keys are released.

This concludes the description of the history of the piano and all of it's components. Understanding each component individually allows for investigations into some of the finer aspects of piano sound production. This thesis will discuss the experiments and modeling conducted to investigate the origins of phantom partials, which are anomalous frequency components found in the sound of the piano. First a description of phantom partials including the history, classical theory, and the results of recent research is presented. This is followed by two plausible theories for the origin of the phantom partials. Then, results of new experiments that lend insight into the origin of these frequency components are described. Finally, a model describing the experimental results is provided along with a discussion of its results in relation to the experimental conditions and conclusions.

Chapter 2

Phantom Partials

Phantom partials are anomalous frequency components identifiable in the sound of the piano. They occur at the sum and difference frequencies of two overtones. For over 30 years, it was widely accepted that these frequency components resulted from the forced-longitudinal motion of the string. [31] However, recent work conducted at Rollins College showed that the string provides minimal contribution to the total power of the phantom partials in comparison to that attributable to the structural components. [32,33] This chapter provides foundational knowledge about phantom partials that will aid in understanding the experiments and model presented in the following chapters.

Every string or set of strings on the piano is tuned to a different fundamental frequency corresponding to a different note of the Western scale. The sound produced when the hammer hits the string is a combination of the fundamental frequency and all of its successive overtones. The fundamental frequency is determined by the speaking length of the string and the wave speed, which is equal to the square root of the ratio of the tension and linear density of the string. In addition to the fundamental frequency, there are overtones that are close to harmonic frequencies found at integer multiples of the fundamental frequency. However, in the piano, the higher overtone frequencies are stretched due to the stiffness of the string and are not harmonics of the fundamental. Thus, the actual frequencies produced

are slightly higher than the true harmonics.

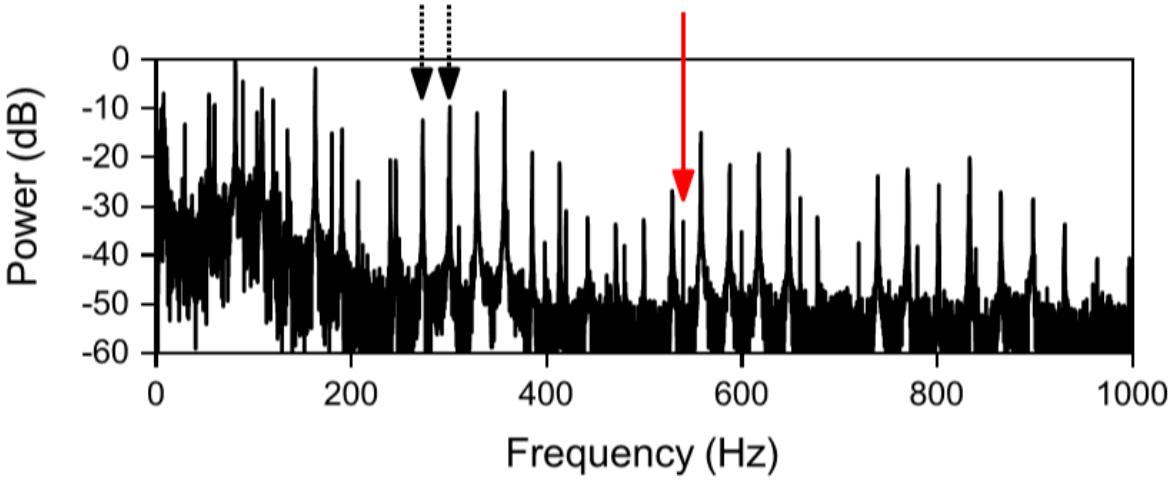

Figure 2.1: An example of a power spectrum for the $B_0^\flat$. The red, solid arrow represents the phantom partial found at the sum of the two overtones marked by the black, dashed arrows.

Because the overtones do not align with the harmonics, it is possible for the sum and difference frequencies of two overtones to also not align with the related overtone of the transverse motion of the string. For example, if the fundamental frequency is 27.5 Hz, the third and fourth harmonics would be identified at 82.5 Hz and 110.3 Hz, respectively. The sum of these frequencies is 192.8 Hz, which is slightly lower than the seventh harmonic found at approximately 193.2 Hz. This effect can be identified in a power spectrum such as the one in Fig. 2.1. In this power spectrum of the $B_0^\flat$ piano string, the two black dashed arrows indicate two successive overtones and their sum is indicated by the red arrow. It is clear that this frequency has a significant amount of power but does not align with any of the other overtones. Bank and Leightnon have demonstrated that these anomalous frequencies can be perceived by a listener and thus are a vital component of the piano sound. [34]

2.1 Historical Context

The first reported identification of these frequency components was by Knoblaugh in 1944 where he referred to them as "clang tones." [35] Knoblaugh attributed these anomolous

frequency components to the hammer strike, which induced a complex motion of the bass bridge. Alfredson and Steinke had a similar idea, that the components were caused by hammer interaction with the string, when they identified them in 1978. [36] Unaware of Knoblaugh's work, Nakaguma and Nakumura identified the partials in 1993 and termed them "secondary partials." [37] However, apparently unaware of all previous work, Conklin identified these components in the piano spectrum and termed them "phantom partials," which remains the common name today. [38] Conklin later attributed these partials to the forced longitudinal motion of the string, and the production of the phantom partials has been generally attributed to a geometric nonlinearity of the string since then. [31]

In the years following Conklin's work, models of the grand piano began to include the generation of these anomalous overtones. The first complete mathematical model of the piano including this effect was published in 2013 by Chabassier, et al. [18] Etchenique, et al. later provided experimental evidence confirming the quadratic dependence of the amplitude of the phantom partial on the amplitude of string vibration that was assumed by Chabassier. [25]

However, work completed in 2017 by Rokni, Neldner, Adkison and Moore demonstrated the significance of components other than the string in the production of phantom partials. [32] Experiments where the bridge of the piano was driven at two frequencies when every string was damped and again when all but one string were damped resulted in nearly the same power in the phantom partial. Further research demonstrated the importance of the structural components of the piano in the generation of the phantom partial. [33] The results of experiments reported in these two journal articles will be elaborated on in a later section.

2.2 Historic Theory of Phantom Partials

We begin our discussion with the commonly accepted theory of phantom partials as of 2015. As previously discussed in Section 1.2.4, two types of longitudinal waves propagate along the string of the piano. The forced-longitudinal waves are most directly associated with

the production of the phantom partials, however, all three wave motions will be considered. [25, 39]

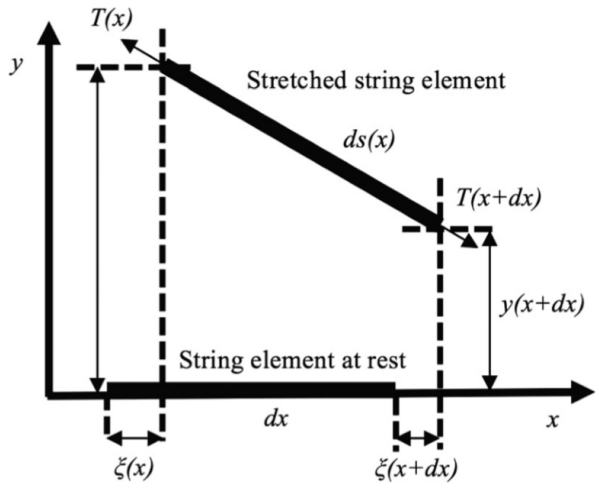

Figure 2.2: Diagram of a string element while at equilibrium and while stretched, after Ref [25].

Fig. 2.2 depicts a small portion of string both at rest and while stretched. At equilibrium, the string has an elemental length of dx, and a corresponding length of $ds(x)$ when stretched by the out of plane displacement. Transverse displacement is represented by y and longitudinal displacement by ξ.

The elemental length dx is infinitesimally small and thus ds can be written as

$$ds = \sqrt{\left(\frac{\partial \xi}{\partial x} + 1\right)^2 dx^2 + \left(\frac{\partial y}{\partial x}\right)^2 dx^2}. \tag{2.1}$$

Changes in the element length will effect the tension in the string, $T(x)$, which is determined by Hooke's law and is given by

$$T(x) = T_0 + ES\left(\frac{ds}{dx} - 1\right), \tag{2.2}$$

where T_0 is the tension of the string at equilibrium, E is Young's modulus, and S is the cross-sectional area of the string. Substituting Eq. 2.1 into Eq. 2.2 and ignoring all higher

order terms results in an expression for the string tension,

$$T \approx T_0 + ES\left[\frac{\partial \xi}{\partial x} + \frac{1}{2}\left(\frac{\partial y}{\partial x}\right)^2\right], \tag{2.3}$$

indicating that the transverse displacement of the string results in a force along the longitudinal direction.

The force per unit length due to the out of plane displacement represents the difference in tension between the two ends of the segment and can be determined by expanding y and ξ as a series of polynomials. This longitudinal force per unit length is given by

$$F_x = ES\frac{\partial^2 \xi}{dx^2} + \frac{ES - T_0}{2}\left[\frac{\partial(\partial y/\partial x)^2}{\partial x}\right]. \tag{2.4}$$

The force acts on a differential mass μdx, where μ is the mass per unit length of string.

Using Newton's second law, Eq. 2.4 can be rewritten as

$$\mu\frac{\partial^2 \xi}{\partial t^2} = ES\frac{\partial^2 \xi}{dx^2} + \frac{1}{2}ES\frac{\partial(\partial y/\partial x)^2}{\partial x}. \tag{2.5}$$

This equation of motion for the longitudinal vibration takes the form of the standard wave equation with an additional force term. The additional force term is a result of the transverse displacement and a second-order nonlinearity. Similarly, the transverse motion wave equation can be derived and written as

$$\mu\frac{\partial^2 y}{\partial t^2} = T_0\frac{\partial^2 y}{dx^2} + \frac{1}{2}ES\frac{\partial}{\partial x}\left(\frac{\partial y}{\partial x}\frac{\partial \xi}{\partial x}\right). \tag{2.6}$$

In this case, the additional force depends on the product of the transverse and longitudinal displacements. Equation 2.6 indicates that the longitudinal and transverse motions are coupled.

To determine the link between the force in the longitudinal direction and the transverse

motion of the string, we assume the normal modes of the string can be approximated by standing waves with zero amplitude at the ends, i.e.,

$$y(x,t) = \sum_{n=1}^{\infty} A_n sin(\omega_n t) sin(k_n x), \tag{2.7}$$

where A_n is the amplitude of the n^{th} mode, ω_n is the angular frequency, k_n is the wave number and t is time. The wave number can be approximated by $k_n = n\pi/L$ for a string pinned at both ends, where L is the speaking length.

For simplicity in understanding the physical system, only two modes, n and m, will be considered. In this case, the transverse motion can be rewritten as

$$y(x,t) = A_n sin(\omega_n t) sin(k_n x) + A_m sin(\omega_m t) sin(k_m x). \tag{2.8}$$

Substituting Eq. 2.8 into the second term of Eq. 2.4 results in an equation for the force per unit length in the longitudinal direction,

$$\begin{aligned} F_{xy} = \frac{-\pi^3(ES - T_0)}{L^3}\Big[& A_n^2 n^3 cos(k_n x) sin(k_n x) sin^2(\omega_n t) \\ & + A_m^2 m^3 cos(k_m x) sin(k_m x) sin^2(\omega_m t) \\ & + \frac{A_n A_m nm}{2}\Big([cos([\omega_n - \omega_m]t) - cos([\omega_n + \omega_m]t)] \times [mcos(k_n x) sin(k_m x) + ncos(k_m x) sin(k_n x)]\Big)\Big] \end{aligned} \tag{2.9}$$

From Eq. 2.9 the sum and difference frequencies of the longitudinal waves induced by transverse motion can be identified as $\omega_n - \omega_m$ and $\omega_n + \omega_m$. Higher harmonics can also be identified but here we only consider the sum and difference frequencies because the harmonics are present in the transverse motion of the string.

Isolating the terms containing sum and difference frequencies, Eq. 2.9 can be written as

$$F_{x,t(+,-)} = \beta_{m,n} A_m A_n \{cos([\omega_n - \omega_m]t) - cos([\omega_n + \omega_m]t)\}, \tag{2.10}$$

where $\beta_{m,n}$ represents all of the constants. Experimental work conducted by Etchenique, et al. experimentally showed the linear relationship between the power in the longitudinal motion and the amplitude of the two driving frequencies indicated by this equation. [25] This linear relationship thus indicates that the amplitude of the longitudinal motion has a quadratic dependence on the string displacement because the amplitudes A_m and A_n are both proportional to the displacement.

2.3 Production in Non-string Components

As indicated in the previous sections, in the decades since the the discovery of phantom partials their origins have been assumed to be in the string. However, the question was asked to N. Etchenique by N. Giordano at an Acoustical Society of America conference, is it possible that some portion of the power in the phantom partial is being generated elsewhere in the piano? At the time, the answer was unknown and prompted researchers at Rollins College to investigate the possibility of other origins. Indeed, Rokni, et al. presented experimental results indicating that there are significant contributions coming from components other than the string. [32]

To investigate the origins of the phantom partials, the experiments reported in Ref. [32] used two electromagnetic shakers that were placed on the soundboard of a 6-foot Steinway grand piano. Each shaker was placed on the underside of the soundboard, one near the bass bridge and one near the edge of the soundboard. The shakers were driven at the second and third overtones of the A_0 string which were approximately the third ($f_3 = 82.5$ Hz) and fourth ($f_4 = 110.3$ Hz) harmonics of the fundamental frequency, 27.5 Hz.

The response of the piano was measured by a one-dimensional accelerometer placed on the soundboard approximately half way between the two shakers at a common antinode of vibration of the two driving frequencies and the sum frequency. Additionally, the shaker driven at the third harmonic was equipped with an impedance head that integrates an

accelerometer and force sensor with the driver.

To determine if the phantom partials are produced only in the string, or if other components also contribute, every string of the piano was damped with the felt dampers attached to the action and strips of cloth. Some strings were additionally damped with pieces of rubber. The A_0 string was damped with three felt blocks wedged between the string and the frame.

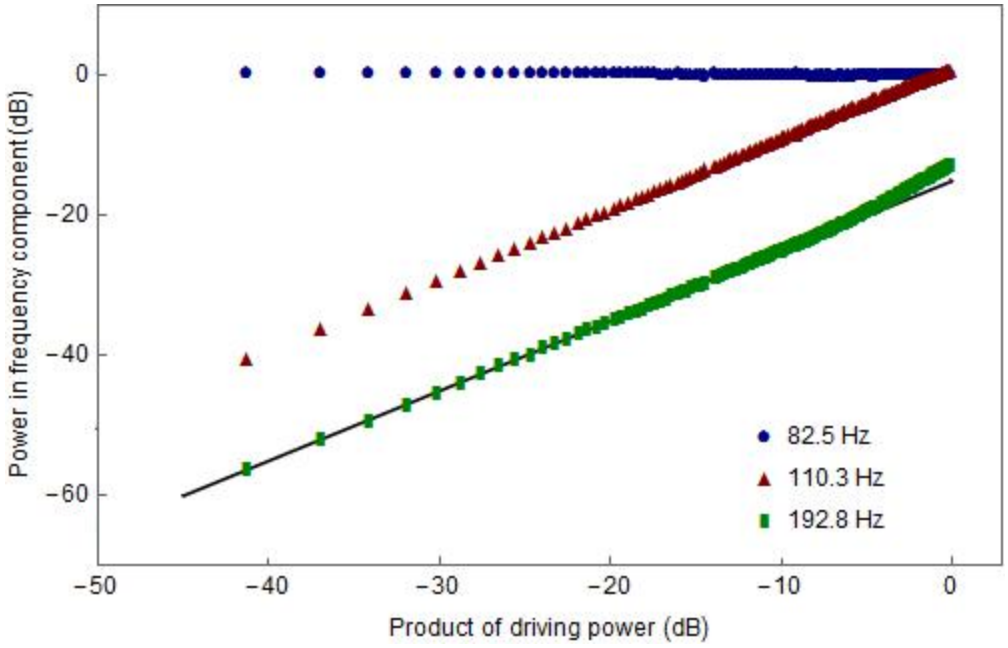

Figure 2.3: Experimental results presented in Ref. [32]. The power in the frequency components are plotted as functions of the product of the driving powers.

During experiments, the shaker driven at f_3 was driven at constant amplitude while the amplitude of the other shaker was linearly increased over a period of 200 s. Figure 2.3 shows the power in the driving frequencies as well as the sum frequency $(f_3 + f_4)$ verses the product of the driving powers. Even with every string damped, there was significant power produced in the sum frequency. Furthermore, to estimate the contribution the string makes to the phantom partial, the experiment was repeated with the felt blocks removed and only the A_0 string was free to vibrate. Figure 2.4 is a plot of the power in the phantom partial verses the product of the driving frequencies for each case. Although there are differences between the results of the two experiments they are minor, indicating that while the string does

contribute to the production of phantom partials, other components make a more significant contribution.

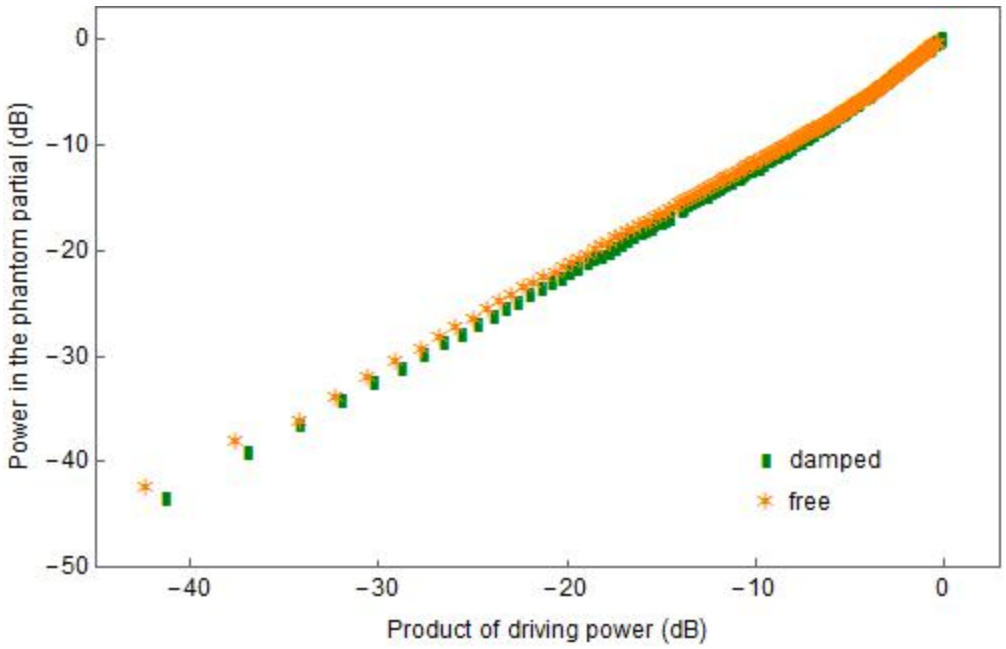

Figure 2.4: Experimental results presented in Ref. [32]. The power in the phantom partial for experimental trials with and without the A_0 string damped are presented as functions of the product of the driving powers.

Moore, Neldner and Rokni extended the experiments reported in Ref. [32] using a similar experimental arrangement. [33] In addition to the accelerometer on the soundboard, two one-dimensional accelerometers were placed on the bridge near the A_0 string. One was placed on the top of the bridge, sensitive to the perpendicular string motion and is referred to as the transverse accelerometer. The other was placed on the side of the bridge, which was sensitive to the motion of the string on axis and is referred to as the longitudinal accelerometer. All strings were damped in a similar matter to the approach described in Ref. [32].

In these experiments two electromagnetic shakers were used to excite motion. However, motion was excited on the bridge, similar to the motion that is induced when the strings move. One shaker was placed on the bridge pin of the A_0 string and driven at f_3. The amplitude of these oscillations were kept constant. The second shaker was placed on the bridge pin of the B_1 string and was driven at f_4 and the amplitude of oscillations were

linearly increased over a period of 200 s. Experiments were conducted once with the A_0 string damped and once with it left free to vibrate. Additionally, to eliminate the possibility of a contact nonlinearity, the experiments were repeated with with acoustic excitation and the results were similar.

Results from the longitudinal accelerometer, shown in Fig. 2.5, indicated that there was more phantom partial generation when the string was free to vibrate, as predicted by historic theory. However, contrary to prior belief, there was also significant phantom partial generation when the string was damped, approximately 20 dB above the noise level, indicating once again that the longitudinal motion is not the sole contributor to their production. Furthermore, the results from both the transverse and soundboard accelerometers showed the same thing. This is not consistent with the theory presented in Section 2.2. From these experiments it can be concluded that the longitudinal motion of the string contributes little to the production of the phantom partials.

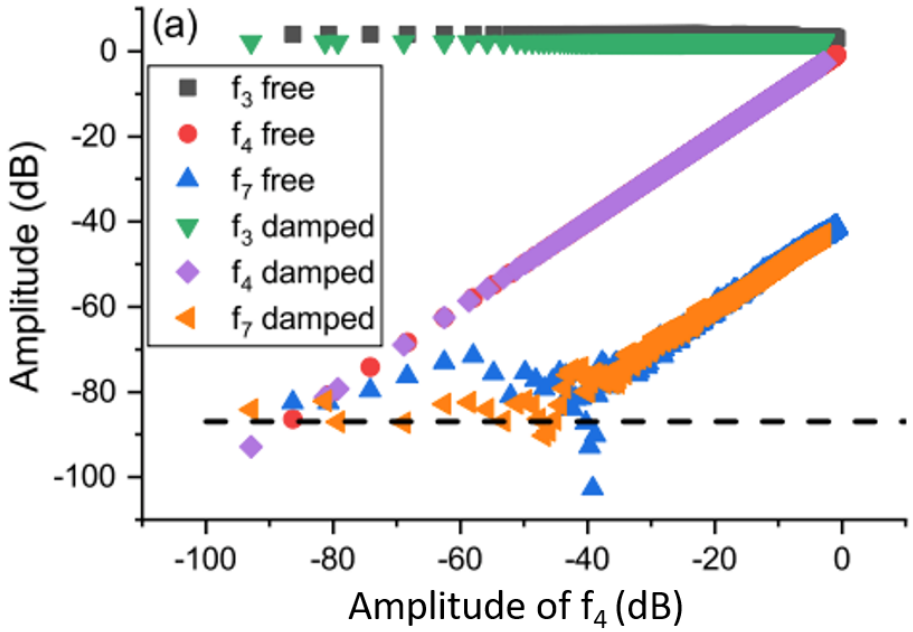

Figure 2.5: Experimental results from Ref [33]. Amplitude in the frequency components of interest are plotted as a function of the amplitude of the fourth harmonic. Results from experiments with the A_0 string damped and left free to vibrate are indicated on the plot and the noise level is indicated by the black dashed line.

This leaves us with the question, if the majority of the power in the phantom partials is not a result of the longitudinal string motion, then what is the origin? The most likely sources are the many wooden components of the piano, such as the soundboard, bridges, case, and ribs. While it is possible that the metal components or glue joints could be responsible for the nonlinearities, these options are less probable. The following chapter will outline two plausible explanations for nonlinear sum frequency generation in the wooden components.

Chapter 3

Two Plausible Theories

The work reported in Ref. [33] leaves the question about what mechanism in the wooden components is generating phantom partials unanswered. This chapter develops the theoretical foundation for two plausible theories that were tested as part of this work and are described in Chapter 4.

3.1 Pressure Induced Nonlinearity

We begin by developing a generic model to describe the possibility that phantom partial generation could be attributable to the nonlinear components of the Young's modulus of wood. Typically, only the linear terms of the Young's modulus are important. However, when materials are bent or stretched by large amounts, the nonlinear components become important and cannot be ignored. Because of the large curvature of the piano soundboard, it would appear that this is a reasonable theory.

Young's modulus E is a measure of elasticity of the material, which is determined by the ratio of stress to strain. [40] Stress σ is defined as the total force F applied to a surface with area A and is given by

$$\sigma = \frac{F}{A}. \tag{3.1}$$

Strain ϵ is defined as the fractional displacement in length dl/l that an object experiences when stress is applied. Stress and strain are related by Young's modulus,

$$\frac{dF}{A} = E\frac{dl}{l}. \tag{3.2}$$

This is one form of Hooke's law that is more typically recognizable in the form $F = -kx$ where k is the spring constant and x is the spring displacement from equilibrium. Hooke's law thus provides a relation between the applied force and how an object will react given intrinsic properties of the material.

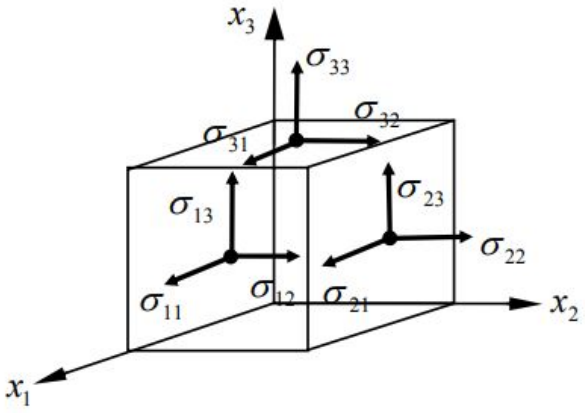

Figure 3.1: Diagram of three dimensional stress components. Image taken from Ref. [41].

It has been shown that Eq. 3.2 can be applied to orthotropic materials such as wood to understand the relation between stress and strain. [42] This results in an elasticity tensor given by

$$\begin{pmatrix} \sigma_1 \\ \sigma_2 \\ \sigma_3 \end{pmatrix} = \begin{pmatrix} E_{11} & E_{12} & E_{13} \\ E_{21} & E_{22} & E_{23} \\ E_{31} & E_{32} & E_{33} \end{pmatrix} \begin{pmatrix} \epsilon_1 \\ \epsilon_2 \\ \epsilon_3 \end{pmatrix}, \tag{3.3}$$

where the shear stresses are ignored. Figure 3.1 is provided as a visualization of the three dimensional stress components that would be found in a piece of wood.

These equations imply linear behavior in materials such as wood and, in many circumstances, can be simplified further to a one-dimensional problem by assuming the off-diagonal elements are zero. This assumption results in Eq. 3.3 becoming

$$\begin{pmatrix} \sigma_1 \\ \sigma_2 \\ \sigma_3 \end{pmatrix} = \begin{pmatrix} E_{11} & 0 & 0 \\ 0 & E_{22} & 0 \\ 0 & 0 & E_{33} \end{pmatrix} \begin{pmatrix} \epsilon_1 \\ \epsilon_2 \\ \epsilon_3 \end{pmatrix}. \tag{3.4}$$

However, this assumption cannot be made when materials are stretched or bent by a large amount. For the common case described by Eq. 3.4 the potential function can be approximated by a parabola, but when stretched pass the linear regime the nonlinear components of Young's modulus become important and this approximation no longer holds. In scenarios where the deflection is large, E in Eq. 3.2 is no longer a constant. Instead, the Young's modulus term is expanded in a Taylor series. This expansion results in each diagonal term becoming a function of strain in the same plane. For example, E_{33} would become $E_{33} + E'_{33}\epsilon_3$, which is a first order approximation for the additional strain and how it modifies the elasticity tensor. Therefore, a term is added that is linear in strain and quadratic in stress.

For example, if we consider a situation in which vibrations are induced in the z direction, represented by the subscript 3, then the strain along the axis of motion becomes

$$\sigma_3 = E_{33}\epsilon_3 + E'_{33}\epsilon_3^2. \tag{3.5}$$

Assuming the motion is driven by two angular frequencies ω_1 and ω_2 with amplitudes A_1 and A_2, we can write the stress along the axis of motion as a function of time t as

$$\epsilon_3 = A_1 cos(\omega_1 t) + A_2 cos(\omega_2 t). \tag{3.6}$$

Squaring this term as indicated by Eq. 3.5 results in

$$\epsilon_3^2 = A_1^2 cos^2(\omega_1 t) + A_2^2 cos^2(\omega_2 t) + A_1 A_2[cos(\omega_1 - \omega_2)t + cos(\omega_1 + \omega_2)t]. \tag{3.7}$$

The sum and difference frequencies can be identified from the last term of this equation.

Within the piano, the force exerted by the string at the fundmental frequency and its harmonics result in stresses. If we consider two of these frequencies, the stress can be written as Eq. 3.6. Therefore, the first two terms in Eq. 3.7 describe the strong higher harmonic generation, which has been identified experimentally in references [32] and [33]. The last term results in the sum and difference frequencies, which also allow us to rewrite the nonlinear strain as

$$\sigma_{nl} = E'_{33}(A_1 A_2[cos(\omega_1 - \omega_2)t + cos(\omega_1 + \omega_2)t]). \tag{3.8}$$

Therefore, a nonlinearity induced by significant applied stress to the soundboard can be modeled by including these nonlinear terms into Eq. 3.4 and could explain phantom partial generation in the piano. This is one theory that was tested experimentally and the results are presented in the next chapter.

3.2 Contact Nonlinearity

Another theory under consideration includes the possibility that nonlinearities are generated at the interfaces between wood pieces. Within the piano there are many of these interfaces, such as the interface between the case and soundboard or the soundboard and the ribs. Additionally, there are thousands of wood-on-wood interfaces in the soundboard as a result of the microscopic cracks in the wood caused by the curvature of the soundboard. Rudenko and Vu have proposed a model for the generation of nonlinearities between two rough surfaces at ultrasonic frequencies and we apply this theory below assuming audible frequencies. [43]

On a microscopic scale, wood is rough and has non-uniform ridges. These ridges will

not align perfectly when two pieces are pressed together and can be modeled by springs of different lengths. Figure 3.2 illustrates this concept where x is the distance between the two pieces.

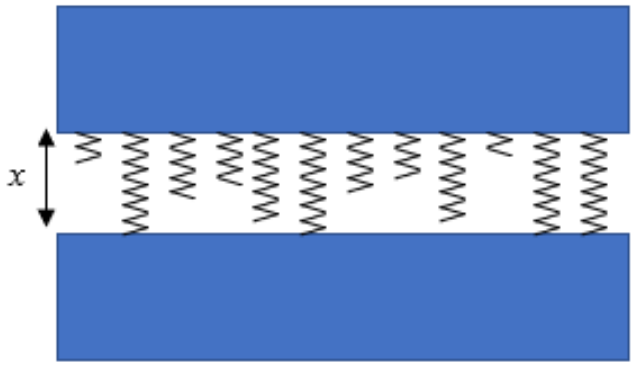

Figure 3.2: Model of two pieces of wood pressed against each other but seperated by a distance x, after Ref [43].

Assuming an ideal spring of length l that obeys Hooke's law, we know that the force F will be proportional to the displacement of the springs from its equilibrium position, $l - x$, with a constant of proportionality given by the spring constant, k. The force, F_i, induced by the i^{th} spring is given by

$$F_i = k(l_i - x)\Theta(l_i - x), \tag{3.9}$$

where Θ is the Heaviside step function. The inclusion of the Heaviside step function is important to ensure that when x is greater than l the force will equal zero, implying that the springs are not in contact with the second surface.

The pressure p is equivalent to the force per unit area so the pressure exerted on the wood by all springs can be determined by

$$p(t) = E\Sigma_i \frac{l_i - x(t)}{l_i}\Theta(l_i - x), \tag{3.10}$$

where E is Young's modulus. Assuming a large number of springs, the summation can be

written as an integral where the total pressure on the interface can be described as

$$p(t) = E \int_{x(t)}^{l_{max}} \frac{l - x(t)}{l} \xi(l) dl, \tag{3.11}$$

where $\xi(l)$ is the distribution of spring lengths and the function is integrated over all spring lengths longer than x.

The equilibrium gap thickness x_0 is the result of static pressure $p = p_0$. Dynamic pressure results in variations in contact thickness such that

$$p = p_0 + \Delta p, \tag{3.12}$$

and

$$x = x_0(p_0) - \Delta x, \tag{3.13}$$

which can be assumed accurate to second order in Δp and Δx. Substituting Eqs. 3.12 and 3.13 into Eq. 3.11, we obtain the relationship

$$\Delta p = \left[E \int_{x_0}^{l_0} \xi(l) \frac{dl}{l} \right] \Delta x + \left[\frac{E}{2} \frac{\xi(x_0)}{x_0} \right] \Delta x^2. \tag{3.14}$$

Notice the nonlinear nature of this equation despite the springs being linear in nature.

This model can be applied to the generation of phantom partials at assuming one plate is driven by two frequencies ω_1 and ω_2 with amplitudes A_1 and A_2 and modeling the distance between the plates as a function of these frequencies,

$$x(t) = x_0 + A_1 cos(\omega_1 t) + A_2 cos(\omega_2 t). \tag{3.15}$$

When this equation is inserted into Eq. 3.14, the output has a term with the same form as Eq. 3.7. The only unknown is the distribution function $\xi(l)$. Using any standard distribution will result in term proportional to the square of the cosine when Eq. 3.11 is evaluated. The

nonlinear change in pressure can be determined when Eq. 3.14 is expanded using Eq. 3.15 and is given by

$$\delta p_{nl} = \frac{E\xi(x_0)}{2x_0} A_1 A_2 [cos(\omega_1 - \omega_2)t + cos(\omega_1 + \omega_2)t]. \tag{3.16}$$

This indicates that any type of linear driving force on one surface will result in nonlinear pressure and the subsequent production of sum and difference frequencies.

The next chapter will describe the experiments conducted to determine if sum frequencies can be produced by either a large amount of stress (Eq. 3.8) or contact between wooden pieces (Eq. 3.16).

Chapter 4

Experiments and Results

Experiments were conducted to determine if a pressure induced nonlinearity or a contact nonlinearity is more likely to produce phantom partials in the wooden components of the piano. Both experiments were conducted on pieces of Sitka spruce to mimic the process occurring in the soundboard. The experiments were conducted on two pieces of wood that were resawed from a single piece of wood. This ensured that the two pieces were as close to identical as possible. The pieces of wood each had dimensions of approximately 54 cm x 22 cm x 0.40 cm. Because the experiments performed were testing for contact nonlinearities, magnets and solenoid drivers were used to induce motion in the board during the experiments. This method allowed for excitation of the board without requiring any direct contact, and therefore any contact nonlinearities can be attributed to wood-on-wood contact.

Measurements were made using one dimensional accelerometers and a laser doppler vibrometer (LDV). The placement of the accelerometer on the face of the board was the point at which the motion at each driving frequency and the sum frequency was maximized. This position was determined using electronic speckle pattern interferometry (ESPI). Two other accelerometers were placed orthogonal to the face of the board on the top and side edges. The LDV was oriented so that velocity measurements were made near the accelerometer on the face of the board.

The resonances of the board were determined by striking the board and calculating a power spectrum of the sound. From this power spectrum, two frequencies with significant power were chosen as the driving frequencies. As a precaution, we ensured that the sum of the two driving frequencies was not equal to a harmonic of either individual driving frequency. This is an important distinction to make, because we are concerned with the production of the sum frequency. If the sum frequency was also equal to a harmonic of one of the driving frequencies, it would be difficult to determine if the power was a result of higher harmonic generation or sum frequency generation.

All experiments were computer controlled using LabView. One program was used to ensure that each electromagnetic driver had the same maximum amplitude for each trial. This was accomplished by sending current through only one solenoid at a time and recording the velocity of the board near the magnet using the LDV. The signal from the LDV was then filtered and integrated to determine the displacement, from which the amplitude of the motion was determined. This was completed for both solenoid and magnet combinations. The driving voltage was adjusted on the amplifiers and pre-amplifiers until the amplitudes of the board motion for each frequency were approximately the same.

A second program was used to perform the experiments and write the results to a file. The input parameters for this program included the total run time for the experiments, the wait time between experiments, sample rate, and the maximum voltage of the drivers. The program repeated the experiment for each of nine trials when the amplitude of each driver was either ramped linearly with time (R), held constant (C), or the driver was completely off (O). The trials therefore are identified as RR, RC, RO, CR, CC, CO, OR, OC, and OO. The program recorded output from the accelerometers, LDV, and force sensor over the total length of each experiment.

A third program integrated the signals collected by the accelerometers and LDV to determine the displacements. These data were then separated into one-second intervals and a harmonic analysis was performed to determine the power in each frequency of interest as a

function of time.

4.1 Pressure experiments

To determine if the phantom partials could be a result of a pressure induced nonlinearity, a wood clamp was used to apply pressure vertically to the board. The piece of Sitka spruce was supported with pieces of oak with a width of 3.77 ± 0.01 cm. The top and bottom edges on both faces of the board were supported completely by oak pieces. The sides were clamped with oak pieces of length 11.3 ± 0.1 cm, which left gaps approximately 1.45 cm wide above and below the top and bottom supports, which gave the board freedom to bend as pressure was applied. A diagram of the experimental configuration is shown in Fig. 4.1. All oak pieces were attached using wood glue and screws. A clamp was used to place pressure over the center of the board and the applied force was measured by a force sensor placed between the wood and the clamp. The board was driven in two locations approximately 11 cm from the top of the board. The location of the magnets and solenoid drivers are indicated in Fig. 4.1. The frequencies of excitation were chosen as $f_1 = 98.8$ Hz and $f_2 = 170.0$ Hz. Therefore, the sum frequency of interest is $f_{1+2} = 268.8$ Hz.

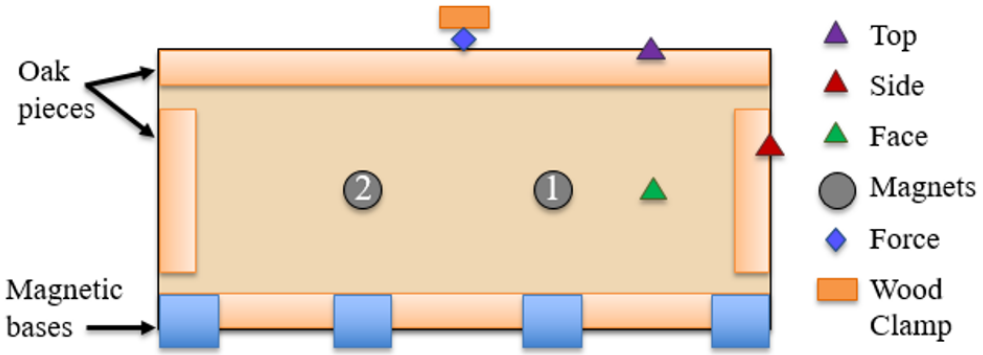

Figure 4.1: Experimental arrangement used to test for pressure induced nonlinearities. Motion in the board was induced at the driving frequencies $f_1 = 98.8$ Hz and $f_2 = 170.0$ Hz, and therefore, the sum frequency of interest was $f_{1+2} = 268.8$ Hz.

To determine if an increase in pressure has any effect on the production of the sum

frequency, the maximum amplitude of the frequency was plotted as a function of the applied force. The results are shown in Fig. 4.2. The first point on the graph refers to the case where approximately no force was applied but still had the clamp in contact with the board. The four trials were conducted with increasing the applied force. It is evident from Fig. 4.2 that the maximum amplitude of the sum frequency occurred when there was no applied force. Every subsequent trial resulted in a reduced maximum amplitude of the sum frequency even though the displacement at the driving frequencies was the same. These results indicate that pressure is not a significant source of the nonlinearity responsible for the production of sum frequencies.

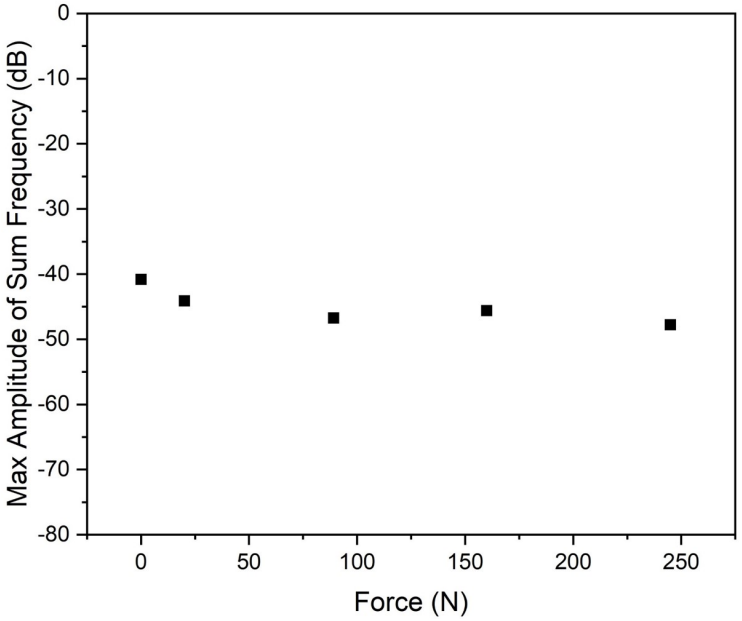

Figure 4.2: Plot of the maximum amplitude of the sum frequency verses the applied force on the board. As the applied force on the wood board is increased, the maximum amplitude of the sum frequency initially decreases and then remains relatively constant.

4.2 Contact experiments

Because adding pressure to the Sitka spruce did not result in an increase in sum frequency generation, the experiment was modified slightly to determine if contact between wooden

pieces can result in an increase in sum frequency generation. To determine how likely it is that this theory accounts for sum frequency generation, a second piece of identical Sitka spruce without an oak border was used. The entire bottom edge was either clamped with aluminum bars or pieces of oak and covered a height of 1.82 cm. These experimental conditions were compared to a control experiment where the bottom edge of the board was only supported by four magnetic bases. Each base had two points of contact with the board, covering an area of approximately 0.98 cm^2 per point of contact. The magnets and solenoid drivers were placed in the upper corners of the board and the accelerometers were kept in approximately the same locations as the previously described experiment. The experimental arrangement is shown in Fig. 4.3.

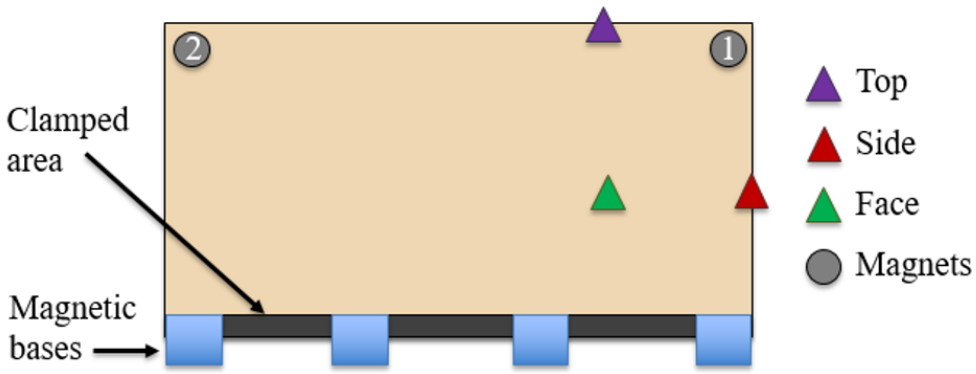

Figure 4.3: Experimental arrangement used to test for contact nonlinearities. Three experiments were conducted when the clamped area was either clamped with pieces of oack, metal bars, or was minimally supported by magnetic bases. Motion was induced in the board at the driving frequencies of $f_1 = 98.8$ Hz and $f_2 = 112.0$ Hz. Thus, the sum frequency of $f_{1+2} = 210.8$ Hz was of interest.

The frequencies of excitation for these experiments were $f_1 = 98.8$ Hz and $f_2 = 112.0$ Hz. Thus, the sum frequency of $f_{1+2} = 210.8$ Hz was of interest. In the first experiment, the clamped region was clamped with pieces of perforated aluminum that were placed on each face of the board and held in place using magnetic bases. Although the metal was not solid, the openings were in the center of the aluminum bar and small enough that the wood can be considered to have been solidly clamped. For the second experiment, the same area was clamped using solid pieces of oak placed on each side of the board and supported with

the magnetic bases. These results were compared to the control test, where the board was supported by the four magnetic bases alone without any additional interface. The magnetic bases were approximately equally spaced during every experiment.

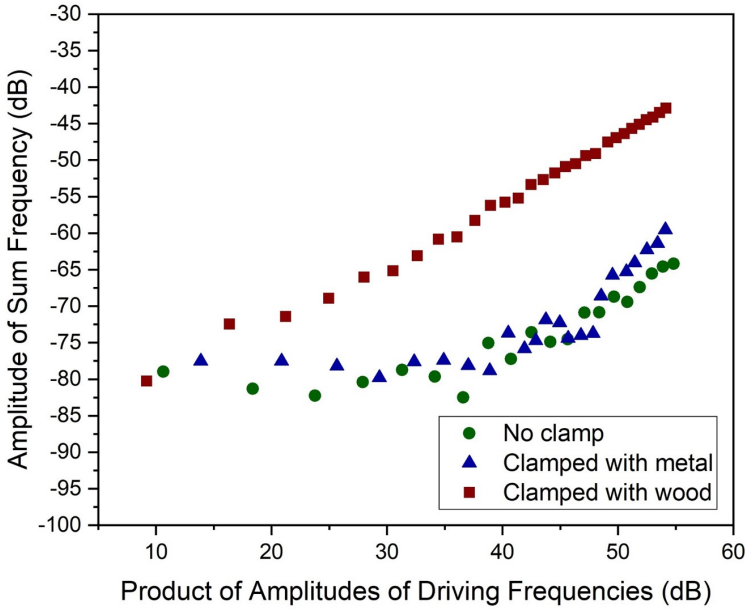

Figure 4.4: Results of experiments testing if a contact nonlinearity could be responsible for nonlinear sum frequency generation. For each experimental variable (wood clamp, metal clamp or no clamp), the amplitude of the sum frequency is plotted as a function of the product of the amplitudes of the driving frequencies.

The results of these experiments are shown in Fig. 4.4, where the amplitude of the sum frequency is plotted as a function of the product of the amplitudes of the driving frequencies for each of the three scenarios. The theory discussed in Chapter 3 suggests that these two quantities can be described by a linear relationship. However, it is clear from Fig. 4.4 that the only experimental condition that resulted in an approximately linear relationship was when the board was clamped with the oak pieces. By comparison, the results from the trials with metal clamping and no clamp do not provide evidence of a linear relationship. Furthermore, the experiments with the wood clamp show efficient sum frequency generation while the other two experiments do not. At the conclusion of the experiments, when the driving amplitudes were at a maximum, the amplitude of the sum frequency produced with the wood clamp was approximately 15 dB higher than the sum frequency amplitude in the

experiment with the metal bars, and approximately 20 dB higher that the sum frequency amplitude with no clamping. These results indicate that contact between wooden pieces is a likely source of sum frequency generation.

4.3 Implications of Experimental Results

Analysis of the results from both experiments, shown in Figs. 4.2 and 4.4, provide plausible evidence that nonlinear sum frequency generation in the wooden components of the piano is more likely a result of wood-on-wood contact than significant amounts of pressure. There has been a significant amount of work using nonlinear acoustics as a tool for non-destructive evaluation (NDE) of materials such as wood and this work can provide insight into the process. Specifically, work by Solodov, et. al. in 2006 describes how contact acoustic nonlinearities (CAN) can result in higher harmonic generation. [44] In the next chapter we present a model based on the theory introduced in Section 3.2 to explain the sum frequency generation when two pieces of wood are in contact.

Chapter 5

Model and Analysis

Two potential theories for nonlinear sum frequency generation in wood were discussed in Chapter 3. The results from the experiments described in the previous chapter clearly indicated that a contact nonlinearity is significantly more likely than a pressure induced nonlinearity to generate sum frequencies. To understand the experimental results, a model based on the theory introduced by Rudenko and Vu was developed and programmed in Mathematica. [43]

5.1 Application of the Model

By normalizing Eq. 3.11 to the length of the longest spring l_{max}, we can rewrite the pressure on the wood interface as

$$\beta(t) = \int_{\eta(t)}^{1} \left(1 - \frac{\eta(t)}{\lambda}\right) \xi(\lambda) d\lambda, \tag{5.1}$$

where $\beta(t) = \dfrac{p(t)}{E}$ is the pressure normalized by Young's modulus, $\eta(t) = \dfrac{x(t)}{l_{max}}$ is the normalized distance between the pieces of wood, and $\lambda = \dfrac{l}{l_{max}}$ is the normalized spring length. The variable $\eta(t)$ can be represented as a function of the driving frequencies ω_1 and

ω_2 with amplitudes A_1 and A_2,

$$\eta(t) = \eta_0 + A_1 sin(\omega_1 t) + A_2 sin(\omega_2 t), \tag{5.2}$$

where η_0 is the equilibrium distance between the pieces of wood.

As noted in Section 3.2, the difficulty of applying Eq. 5.1 is that the distribution function $\xi(\lambda)$ is unknown. We begin with the simplest case where all spring lengths are equally probable. We represent this scenario with a linear distribution with a constant slope such that $\xi(\lambda) = 1$. Figure 5.1 provides a graphical representation of the distribution. While this is unlikely to represent the complex rigidness of wood, it provides a baseline to compare to the results using other distribution functions. When this distribution function is inserted into Eq. 5.1, the result of the integration is

$$\beta(t) = 1 - \eta(t) + \eta(t) ln[\eta(t)]. \tag{5.3}$$

Equation 5.3 is used to model the experiments described in Section 4.2 where the driving frequencies are given by $f_1 = 98.8$ Hz and $f_2 = 112$ Hz. Therefore, a test scenario requires that the amplitude of the first driving frequency is linearly ramped over time ($0 < A_1 < A_{max}$) while the amplitude of the second driving frequency is held constant ($A_2 = A_{max}$). One important thing to note is that the total separation between the two pieces of wood was restricted to between 0 and 1. Therefore, η_0 was required to be greater than the sum of the amplitudes A_1 and A_2, and $A_1 + A_2 + \eta_0 < 1$.

The program produced results similar to those found in Ref. [33], where the power in the frequency components is plotted as a function of the power in the ramped frequency. This was accomplished by generating a table that iterates time from 0 to 10 in increments of 0.001. Then, a **Do** loop generates a power spectrum for the whole time interval for driving frequency amplitudes increasing in 120 equal increments from 0 to A_{max}. For each power spectrum generated, the value of the maximum amplitude of each frequency of interest was

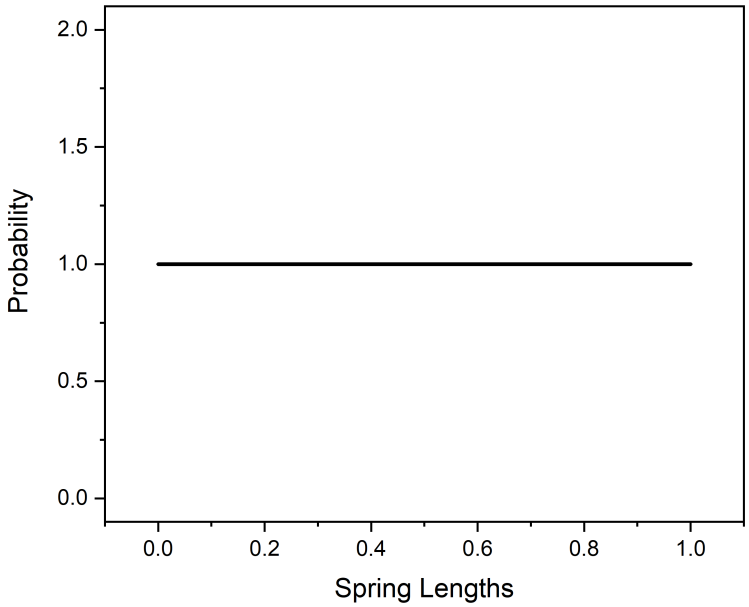

Figure 5.1: A constant distribution function representing $\xi(\lambda) = 1$ depicts a scenario where every spring length is equally probable.

stored in a table. Finally, to determine the best fit for the model, parameters such as η_0 were adjusted using an additional **Do** loop until the best fit using the least squares method was achieved. All trials had an η_0 range from 0.02 to 0.98 in increments of 0.01.

An arbitrary value for A_{max} was set at 0.01, or one one-hundredth of the longest spring length. This value was chosen as an initial guess because it seems likely that at the large wood-on-wood interfaces in the piano, the amplitudes of vibration would be very small. However, for future research, we purpose that the code is modified and allow for the value of A_{max} to vary over a larger range until a best fit is achieved.

For the constant distribution function, it was found that the best fit to the experimental data was achieved when η_0 was equal to 0.37. The results of this model are shown in Fig. 5.2 where both the amplitudes of the frequency components for theory (lines) and experimental data (points) are plotted as a function of the amplitude of the first driving frequency.

The results from this distribution function depicted in Fig. 5.2 are surprising considering

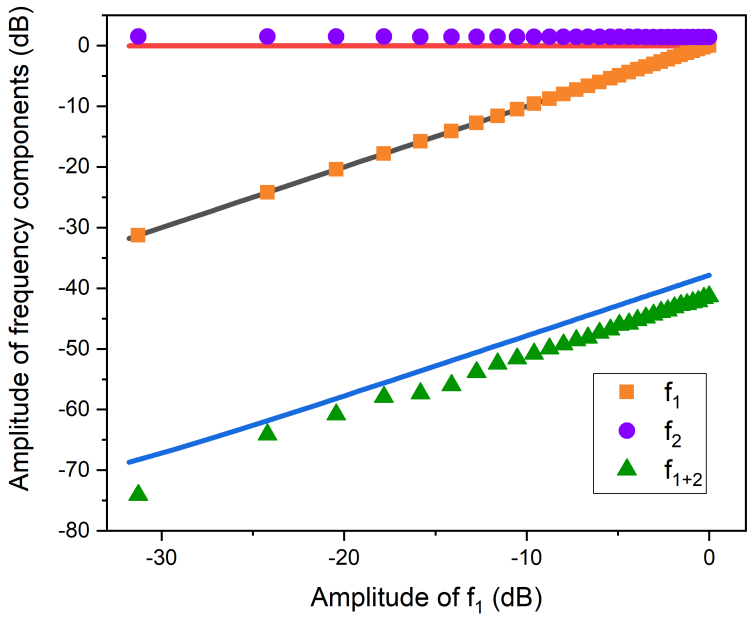

Figure 5.2: Results from the model assuming a distribution where all spring lengths are equally probable are depicted by the solid lines and are plotted with the experimental results described in Section 4.2. Amplitudes of each frequency component are plotted as a function of the amplitude of the ramped driving frequency. The maximum amplitude of the driving frequencies was 0.01 and the equilibrium distance between the pieces of wood η_0 was equal to 0.37.

the unlikeliness of this particular distribution function, however, they are promising since a reasonable fit was achieved with a small driving amplitude. For this particular distribution function, we were able to identify that the model generates a similar amount of amplitude in the sum frequency to that measured during experimentation when just over one third of the ridges are initially in contact with the second piece of wood.

Because the results with a constant distribution were promising, we then repeated the process using a slightly more advanced model. In this case, we have given the linear distribution function some slope and we represent it as

$$\xi(\lambda) = \frac{1}{2}\lambda + \frac{1}{2}. \tag{5.4}$$

In this case, the distribution function represents a scenario where longer ridges are more likely that short ridges. The distribution function is represented in Fig. 5.3 which displays the probability of each spring length. We note that any slope or y-intercept could have been chosen, but for preliminary determination of the feasibility of the model, these values are not critically important and could be modified as part of future work.

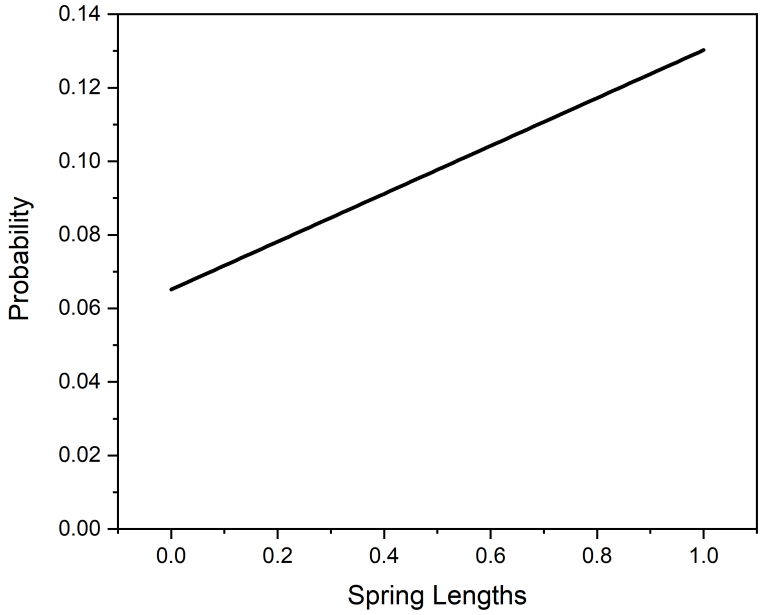

Figure 5.3: For a linear distribution represented by Eq. 5.4, the probability of each spring length is given.

When Eq. 5.4 is substituted into Eq. 5.1 and the integration is performed, the resultant function is given by

$$\beta(t) = 0.75 + \left[\frac{\eta(t)}{4} - 1\right]\eta(t) + \frac{\eta(t) ln[\eta(t)]}{2}. \tag{5.5}$$

The same modeling process was repeated for this distribution. The maximum amplitude of the driving frequencies was again $A_{max} = 0.01$ and the best fit to the data was when the equilibrium distance between the pieces of wood η_0 was equal to 0.33. Thus in this case, the best fit corresponds to when one third of the ridges are initially in contact. The results of

this model are shown in Fig. 5.4 where both the amplitudes of the frequency components for the theory (lines) and experimental data (points) are plotted as a function of the amplitude of the first driving frequency.

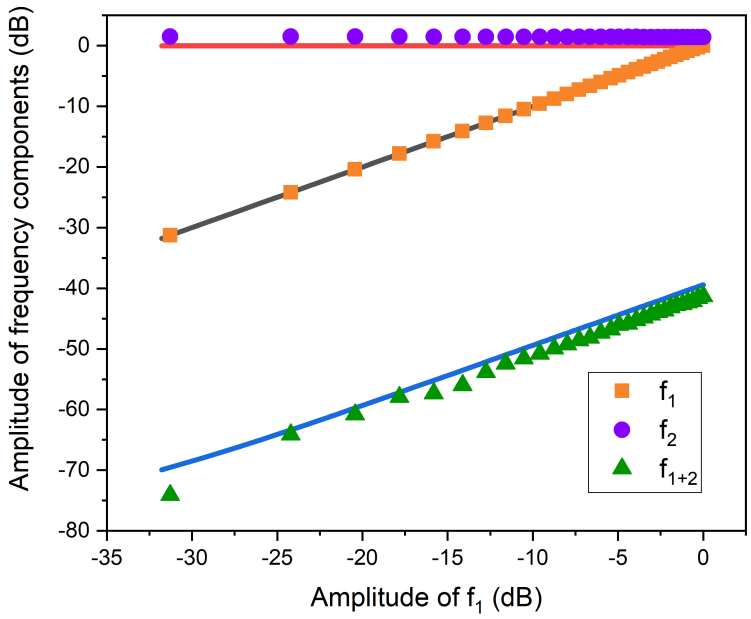

Figure 5.4: Results from the model with a distribution function given by Eq. 5.4. The maximum amplitude of the driving frequency was 0.01 and the equilibrium distance between the pieces of wood η_0 was 0.33.

Similar to the constant distribution, the linear distribution with some slope resulted in a reasonable fit to the experimental data collected. Although this distribution function is still unlikely, once again the results for the model are promising since we can identify parameters that result in similar sum frequency production as the experiments conducted.

Finally, we test the model using a distribution function that is slightly more probable. Because wood is rigid, it is likely that the distribution of the heights of the microscopic ridges will peak somewhere between the maximum and minimum spring lengths. One possible model for this type of distribution is a Lorentzian profile. In the simplest case, the spring length is assumed to be one-half of the maximum spring length such that the distribution is

given by,

$$\xi(\lambda) = \frac{b}{\left(\lambda - \frac{1}{2}\right)^2 + b^2}, \tag{5.6}$$

where b is the full-width at half-maximum (FWHM) of the distribution function. Figure 5.5 depicts this scenario where there is a peak in the probability of ridges around some central length and the probability of shorter or taller ridges is much less.

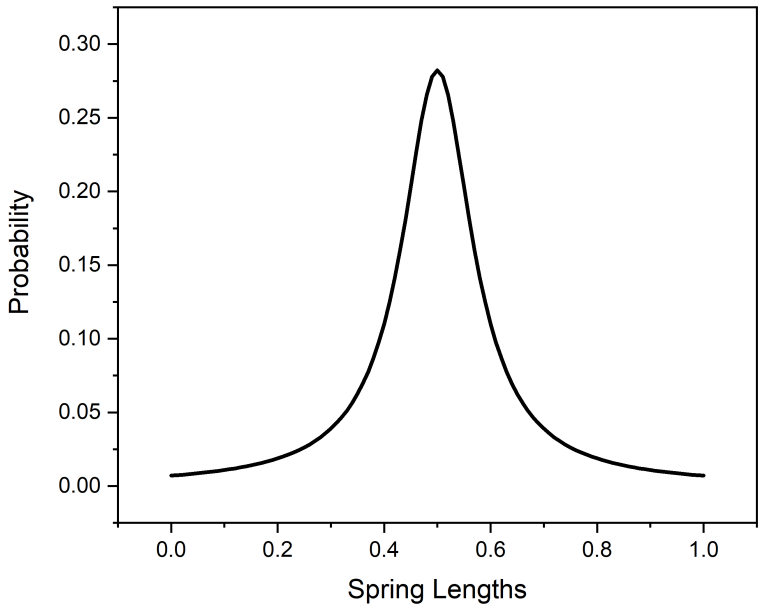

Figure 5.5: A Lorentzian distribution based on Eq. 5.6 will result in a larger probability for spring lengths near the center of the distribution than near the tails.

Inserting Eq. 5.6 into Eq. 5.1 and performing the integration results in a function for

the normalized pressure given by

$$\beta(t) = \left(\frac{1}{2cot^{-1}(2b)}\right) \Big(cot^{-1}\left[\frac{2b}{1-2\eta(t)}\right] + cot^{-1}[2b] - \frac{2\eta(t)}{(1+4b^2)}\Big[tan^{-1}\left[\frac{1}{2b}\right] + tan^{-1}\left[\frac{1-2\eta(t)}{2b}\right] + b(ln[4b^2+(1-2\eta(t))^2] - 2ln[\eta(t)] - ln[1+4b^2])\Big]\Big), \tag{5.7}$$

where the integration was performed in Mathematica.

The added complexity of the Lorentzian distribution also adds another variable, b. To compare the different distribution functions, the value for A_{max} was kept the same at 0.01, but an additional **Do** loop was added to the code to determine the best combination of b and η_0 values. Several test trials indicated that a b range of 0.05 to 0.15 yielded results consistently close to matching the experimental results. This also follows the logic that if the ridges on wood vary in length, the variation is probably minimal. The best fit with this distribution function was determined to be $b = 0.08$ and $\eta_0 = 0.98$. The results of this simulation are shown in Fig. 5.6.

This distribution function produced the closest fit to the experimental data, however the η_0 was significantly different. A value of 0.98 indicates that the best fit is achieved when almost all ridges are initially in contact with the second board.

It was also identified during this modeling test that sum frequency generation is greatly influenced by the η_0 value. Because changing the initial distance between the pieces of wood η_0 has such a big impact on the fitting of each distribution function, a different code was used to determine the effect of changing η_0. In this code both A_1 and A_2 were held at a constant amplitude of 0.01. This code loops over all possible values for η_0 from 0.02 to 0.98 in increments of 0.01 and determines the maximum amplitude of the sum frequency. This allows us to identify what happens to the production of the sum frequency as the equilibrium displacement is changed. The first two cases with linear distribution functions

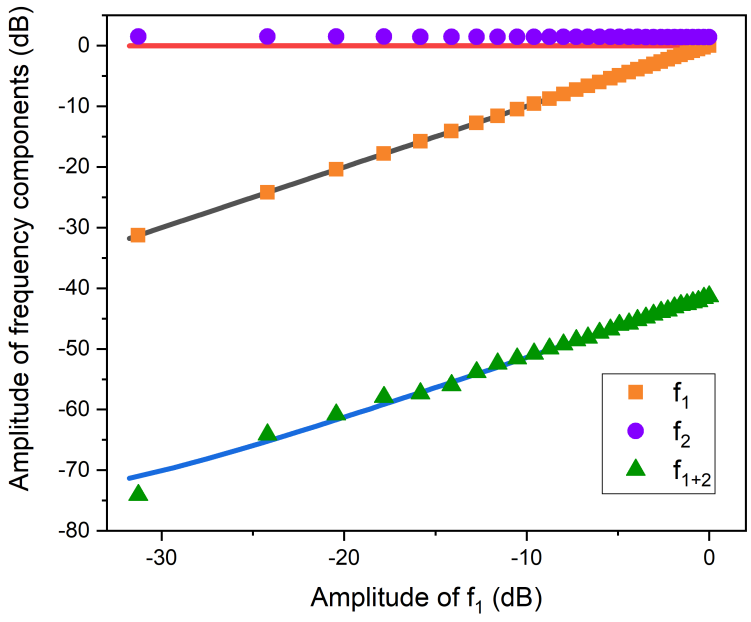

Figure 5.6: Results from the model with a Lorentzian distribution plotted with the experimental results described in Section 4.2. The maximum amplitude for both driving frequencies was 0.01, the FWHM b was 0.08, and the equilibrium distance between the pieces of wood η_0 was 0.98.

resembled normal logarithmic decay curves and did not provide significant insight. However, the results produced from this model using the Lorentzian distribution were quite interesting and are shown in Fig. 5.7.

Figure 5.7 indicates that with an η_0 value slightly less than the value in which the distribution function is centered will result in the maximum sum frequency generation. An η_0 value slightly greater than the center of the distribution results in the least sum frequency generation. However, because we are trying to model experimental data, the results shown in Fig. 5.6 indicated that there should be five values for η_0 in which a good fit to the data is achieved. The initial model determined the best fit by identifying the parameter with the smallest least squares error. Further investigations will need to be conducted to identify if each of these five points could be said to provide a good fit and what that means for comparing to physical parameters.

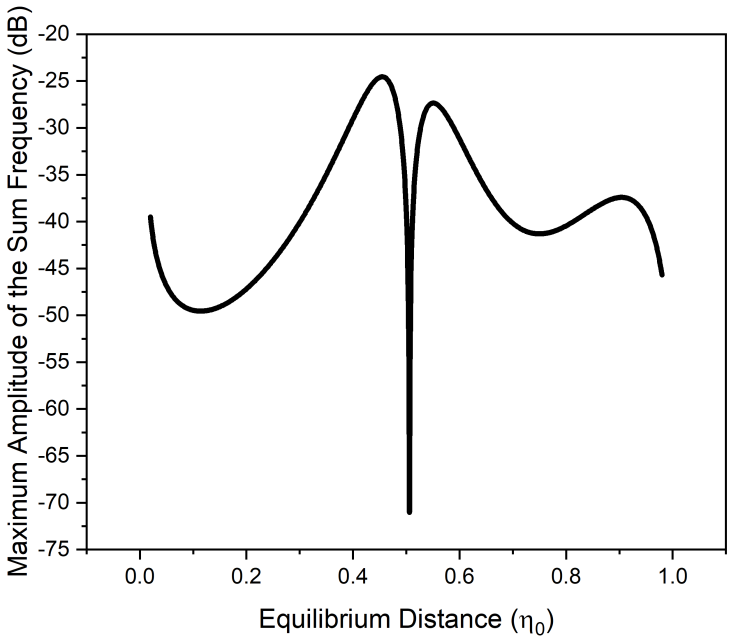

Figure 5.7: The predicted maximum amplitude of the sum frequency when a Lorentzian distribution is assumed is plotted as a function of the equilibrium distance between the pieces of wood. The maximum amplitude of the driving frequencies is 0.01 and the FWHM is 0.08.

5.2 Analysis

The model described in Section 5.1 appears to model the experiments conducted with the wood-on-wood interface, however, there are some major differences. In the experimental arrangement, only a small portion of the board, around 8% of the area on each face was clamped. In contrast, the model works under the assumption that the whole area of the board is clamped. The model also works under the assumption that the board is driven where the pieces of wood are in contact and that this is where all measurements are recorded. However, in the experiments, the board is driven in the upper corners and measurements were recorded in the locations with the most motion based on inspection of ESPI images.

This does not necessarily mean that the model has no merit in the situation. If we continue to work under the assumption that most of the nonlinearity is produced at these wooden interfaces, then we can argue that the portion of the board that is not clamped adds

minimal contribution to the production of sum frequencies, but does move in response to the clamped area and thus provides information about how the clamping effects the power in each frequency component.

Another interesting aspect to note from Fig. 5.7 is how dependent the model is on the equilibrium distance between the pieces of wood. This indicates that there is some aspect of static pressure that is important. In the experiments described in Section 4.1 pressure was applied vertically onto the piece of sitka spruce. This resulted in slight curvature of the board and could have resulted in production of sum and difference frequencies according to Eq. 3.5, but as shown in Fig. 4.2 it is unlikely to be the source of phantom partial generation in the piano.

However, the experiments described in Section 4.2 also used pressure to hold the pieces of oak and metal onto the board. While the process to set-up the experiments was similar for each experiment, variations in the pressure holding the pieces together could have effected the production of sum frequencies. This is identifiable in both Fig. 5.7 and from post-experiment checks where the ESPI generated images of the modal structures varied slightly between the same set-ups. This is something that needs to be investigated in the future to determine the overall effect of slight variations in the clamping pressure on the pieces of wood on the experimental and theoretical findings. We purpose repeating the experiments described in Section 4.2 with the addition of flat force sensors placed between the piece of Sitka spruce and the pieces of wood or metal to ensure equal pressure across all experiments.

Despite these concerns, the ability to fit the model to the data using several different distribution functions is promising. It appears that the most important aspects for curve fitting were small maximum driving amplitudes and allowing the equilibrium distance between the pieces of wood to shift rather than determining the correct distribution of the ridge heights.

Chapter 6

Conclusions

In the previous chapters we have discussed the possibility of phantom partial generation in the wooden components of the piano. Having first presented both the history of the piano and the historical knowledge of phantom partials, we then presented two plausible theories that could explain how sum frequencies are generated in the wooden components of the piano. Experimental results were presented that tested the possibility of each theory followed by results from the model based on the theory describing wood-on-wood contact.

The experimental results indicate that it is more likely that sum frequency generation results from wood-on-wood contact rather than internal stress. Having stress on the board did result in sum frequency generation above the noise level, but it is unlikely that this was a result of pressure. It is more likely that the nonlinearity was a result of the wood-on-wood contact from the edge pieces used to keep the board from bending.

In contrast, experimental results of experiments where the piece of Sitka spruce was clamped with either wood or metal only showed strong sum frequency generation when clamped with wood. While metal clamping and a free board did result in sum frequency generation, it was minimal compared to the results from experiments when the edge of the board was clamped with wood.

The experimental results with the wood-on-wood contact were then compared to a model

based on a theory that we derived from Rudenko and Vu. [43] While the model does not represent the experimental arrangement perfectly, we argue that it resembles the experiment closely enough that we are able to draw some broad conclusions. The first important conclusion from the modeling is that several distribution functions for the spring lengths can be modified to fit the measurements by adjusting the maximum amplitude of the drivers and allowing the equilibrium distance between the pieces of wood to vary until the best fit is achieved. Second, it appears that the nonlinearity is critically dependent on the pressure applied to the joint. This is most explicitly identifiable in Fig. 5.7, where the difference in η_0 from the maximum sum frequency generation to the least sum frequency generation is less than 0.1. While we do not have an explanation for this extreme sensitivity, we purpose it as possible future research. However, within the scope of this thesis, we conclude that the theory that phantom partials are generated at the wood-on-wood interfaces in the piano is plausible.

Despite this promising conclusion, there are still many questions that have yet to be answered. Although we have evidence that a significant amount of phantom partial generation is coming from the wooden components, we do not know which wooden structure or interface in the piano contributes the most. Furthermore, it was out of the purview of this work to investigate the effect of glue joints have on the production of sum frequencies. We hypothesize that the model will still be valid even with the addition of glue binding, but this is something that will need to be investigated in future works.

Nevertheless, we have made significant advancements in identifying the origins of phantom partials in the piano. It is clear that the strings contribute very minimally to the production of phantom partials, which means that most of power in the frequency components must be produced in the structural components. Experimentation has provided no significant evidence that any of the non-wooden parts of the structure, such as the metal frame, are contributing significant power. Furthermore, if phantom partial generation is a result of cracks in the wood, we would have expected to find an increase in the amplitude

of the phantom partial as the applied pressure on the board was increased, however, this was not the case. On the other hand, there was significant phantom partial generation when two pieces of wood were placed in contact. This strongly indicates that phantom partial generation in the piano is likely a result of the nonlinearities generated at wood-on-wood interfaces.

Bibliography

[1] M. Campbell, *Musical instruments: history, technology, and performance of instruments of western music*. New York: Oxford University Press, 2004.

[2] N. Giordano, *Physics of the Piano*. New York: Oxford University Press, 2016.

[3] "Parts of a Piano (Grand and Upright Piano Diagrams)." `https://www.homestratosphere.com/piano-parts/`, 2019.

[4] H. A. Conklin, "Design and tone in the mechanoacoustic piano . Part I . Piano hammers and tonal effects," *The Journal of the Acoustical Society of America*, vol. 99, pp. 3286–3296, 1996.

[5] H. A. Conklin, "Design and tone in the mechanoacoustic piano . Part II . Piano structure," *The Journal of the Acoustical Society of America*, vol. 100, pp. 695–708, 1996.

[6] H. A. Conklin, "Design and tone in the mechanoacoustic piano . Part III . Piano strings and scale design," *The Journal of the Acoustical Society of America*, vol. 100, pp. 1286–1298, 1996.

[7] H. A. Conklin, "Piano design factors - their influence on tone and acoustical performance," in *Five Lectures on the Acoustics of the Piano*, (Stockholm, Sweeden), 1990.

[8] J. J. Tan, A. Chaigne, and A. Acri, "Operational transfer path analysis of a piano," *Applied Acoustics*, vol. 140, pp. 39–47, 2018.

[9] A. Chaigne, B. Cotte, and R. Viggiano, "Dynamical properties of piano soundboards," *The Journal of the Acoustical Society of America*, vol. 133, no. 4, pp. 2456–2466, 2013.

[10] T. R. Moore and S. A. Zietlow, "Interferometric studies of a piano soundboard," *The Journal of the Acoustical Society of America*, vol. 119, no. 3, pp. 1783–1793, 2006.

[11] H. Suzuki, "Vibration and sound radiation of a piano soundboard," *The Journal of the Acoustical Society of America*, vol. 80, no. 6, pp. 1573–1582, 1986.

[12] J. Kindel and I.-C. Wang, "Modal Analysis and Finite Element Analysis of a Piano Soundboard," in *5th International Modal Analysis Conference*, (London, England), pp. 1545–1549, 1987.

[13] N. Giordano, "Simple model of a piano soundboard," *The Journal of the Acoustical Society of America*, vol. 102, pp. 1159–1168, 1997.

[14] N. Giordano, "Mechanical impedance of a piano soundboard," *The Journal of the Acoustical Society of America*, vol. 103, no. 4, pp. 2128–2133, 1998.

[15] J. Berthaut, M. N. Ichchou, and L. Jezequel, "Piano soundboard: structural behavior, numerical and experimental study in the modal range," *Applied Acoustics*, vol. 64, pp. 1113–1136, 2003.

[16] K. Ege, X. Boutillon, and M. Rebillat, "Vibroacoustics of the piano soundboard: (Non) linearity and modal properties in the low- and mid-frequency ranges," *Journal of Sound and Vibration*, vol. 332, pp. 1288–1305, 2013.

[17] X. Boutillon and K. Ege, "Vibroacoustics of the piano soundboard: Reduced models, mobility synthesis, and acoustical radiation regime," *Journal of Sound and Vibration*, vol. 332, no. 18, pp. 4261–4279, 2013.

[18] J. Chabassier, A. Chaigne, and P. Joly, "Modeling and simulation of a grand piano," *The Journal of the Acoustical Society of America*, vol. 134, pp. 648–665, 2013.

[19] R. Corradi, S. Miccoli, G. Squicciarini, and P. Fazioli, "Modal analysis of a grand piano soundboard at successive manufacturing stages," *Applied Acoustics*, vol. 125, pp. 113–127, 2017.

[20] B. Trevisan, K. Ege, and B. Laulagnet, "A modal approach to piano soundboard vibroacoustic behavior," *The Journal of the Acoustical Society of America*, vol. 141, pp. 690–709, 2017.

[21] N. Giordano and A. J. Korty, "Motion of a piano string : Longitudinal vibrations and the role of the bridge," *The Journal of the Acoustical Society of America*, vol. 100, pp. 3899–3908, 1996.

[22] R. E. Kirk, "Tuning Preferences for Piano Unison Groups," *The Journal of the Acoustical Society of America*, vol. 31, no. 12, p. 1644, 1959.

[23] G. Weinreich, "Coupled piano strings," *The Journal of the Acoustical Society of America*, vol. 62, no. 6, pp. 1474–1484, 1977.

[24] H. Fletcher, "Normal Vibration Frequencies of a Stiff Piano String," *The Journal of the Acoustical Society of America*, vol. 36, no. 1, 1964.

[25] N. Etchenique, S. R. Collin, and T. R. Moore, "Coupling of transverse and longitudinal waves in piano strings," *The Journal of the Acoustical Society of America*, vol. 137, pp. 1766–1771, 2015.

[26] P. M. Morse and K. U. Ingard, *Theoretical Acoustics*. New York: McGraw-Hill, 1968.

[27] I. Nishiguchi, "Recent research on the acoustics of pianos," *Acoustical Science and Technology*, vol. 25, no. 6, pp. 413–418, 2004.

[28] D. E. Hall and A. Askenfelt, "Piano string excitation V : Spectra for real hammers and strings," *Journal of the Acoustical Society of America*, vol. 83, no. 4, pp. 1627–1638, 1988.

[29] A. Askenfelt and E. V. Jansson, "From touch to string vibrations. iii: String motion and spectra," *The Journal of the Acoustical Society of America*, vol. 93, no. 4, pp. 2181–2196, 1993.

[30] S. Birkett, "Experimental investigation of the piano hammer-string interaction," *The Journal of the Acoustical Society of America*, vol. 133, no. 4, pp. 2467–2478, 2013.

[31] H. A. Conklin, "Generation of partials due to nonlinear mixing in a stringed instrument," *The Journal of the Acoustical Society of America*, vol. 105, no. 1, pp. 536–545, 1999.

[32] E. Rokni, L. M. Neldner, C. Adkison, and T. R. Moore, "The production of phantom partials due to nonlinearities in the structural components of the piano," *Journal of the Acoustical Society of America*, vol. 142, no. 4, pp. EL344–EL349, 2017.

[33] T. R. Moore, L. M. Neldner, and E. Rokni, "Structural contributions to phantom partial generation in the piano," *Journal of the Acoustical Society of America*, vol. 144, no. 3, pp. 1564–1571, 2018.

[34] B. Bank and H.-M. Lehtonen, "Perception of longitudinal components in piano," *The Journal of the Acoustical Society of America*, vol. 128, no. 3, pp. EL117–EL123, 2010.

[35] A. F. Knoblaugh, "The Clang Tone of the Pianoforte Published by the Acoustical Society of America," *The Journal of the Acoustical Society of America*, vol. 16, p. 102, 1944.

[36] R. J. Alfredson and S. Steinke, "Fourier Transform Methods for Analysing the Sounds of a Piano," *Acoustica*, vol. 39, pp. 130–132, 1978.

[37] I. Nakamura and D. Naganuma, "Characteristics of piano sound spectra," in *Proc. Stockholm Music Acoust. Conf. 1993* (A. Friberg, J. Iwarsson, E. Jansson, and J. Sundberg, eds.), (Stockholm, Sweeden), pp. 325–330, 1993.

[38] H. A. Conklin, "Piano strings and " phantom " partials," *The Journal of the Acoustical Society of America*, vol. 102, no. 659, pp. 1996–1997, 1997.

[39] B. Bank and L. Sujbert, "A Piano Model Including Longitudinal String Vibrations," in *Proc. of the 7th Int. Conference on Digital Audio Effects*, (Naples, Italy), pp. 89–94, 2004.

[40] J. R. Taylor, *Classical Mechanics*. University Science Books, 2005.

[41] P. Kelly, "7.2 Analysis of Three Dimensional Stress and Strain," in *Solid mechanics - part II Lecture Notes*, pp. 201–219, 2015.

[42] S. Holmberg, K. Persson, and H. Petersson, "Nonlinear mechanical behaviour and analysis of wood and fibre materials," *Computers and Structures*, vol. 72, pp. 459–480, 1999.

[43] O. V. Rudenko and C. A. Vu, "Nonlinear Acoustic Properties of a Rough Surface Contact and Acoustodiagnostics of a Roughness Height Distribution," *Acoustical Physics*, vol. 40, no. 4, pp. 593–596, 1994.

[44] I. Solodov, K. Pfleiderer, and G. Busse, "Nonlinear Acoustic NDE Using Complete Nonclassical Spectra," in *Innovations in Nonlinear Acoustics: 17th International Symposium on Nonlinear Acoustics* (A. A. Atchley, V. W. Sparrow, and R. M. Keolian, eds.), pp. 35–42, American Institute of Physics, 2006.